Optics & Laser Technology 158 (2023) 108886

Contents lists available at ScienceDirect

Optics and Laser Technology

journal homepage: www.elsevier.com/locate/optlastec

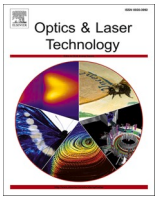

Microstructures formed in polypropylene by a single pulse of near-infrared ultrafast laser with nonlinear absorption

Arifur Rahaman, Aravinda Kar

CREOL, The College of Optics & Photonics, University of Central Florida, Orlando, FL 32816, USA

ARTICLE INFO

Keywords:
Ultrafast laser
Polymers
Nonlinear absorption
Ring-shaped microstructure
Void morphology

ABSTRACT

Polymeric materials are expected to interact with lasers differently depending on the presence of impurities in the material since the impurities can induce different absorption mechanisms. Especially ultrafast lasers of near-infrared wavelength may exhibit linear absorption at low intensities, but nonlinear absorption is found to occur at higher intensities. Two types of polypropylene samples, one containing impurity and the other relatively pure, are examined in this study for the nonlinearity in their absorption characteristics at a near-infrared wavelength. The absorptances of the samples are determined by measuring their optical properties, i.e., reflectance, transmittance, and the multiphoton excitation order is determined by considering a nonlinear intensity model for the propagation of the laser beam through the samples. In addition, the self-phase modulation of the laser is found to enhance the absorption mechanism by switching the absorption from the nonresonant to resonant mode. These variations in the absorption mechanisms can induce different damage features as observed in the polypropylene samples.

1. Introduction

The interaction of intense ultrafast laser pulses with materials leads to different scientific and industrial applications based on laser materials processing. Polymer is the first material which was processed with an ultrafast laser in 1987 by Srinivasan et al. [1], and Kuper and Stuke [2]. These two studies showed damage-free clean surface in PMMA (polymethyl methacrylate) after ablation using femtosecond (fs) ultraviolet (UV) excimer lasers, where the ablation threshold was significantly lower than previously studied ablation using nanosecond (ns) lasers [3,4]. Ultrafast laser ablation can also reduce the heat-affected zone (HAZ) in high conductivity materials such as metals [5]. Ultrafast laser pulses enable depositing energy on materials at much shorter time scales than the time for thermal diffusion in the material, resulting in laser-material interactions with minimal thermal effect [6]. Considerable studies have been conducted to harness this unique characteristic of ultrafast laser beams for achieving thermal damage-free processing of materials for numerous applications such as drilling [7], cutting [8], surface hardening [9], polishing [10], cleaning [11], and micro/nano-machining [12,13]. Zhao et al. [7] studied drilling of transparent glass using a fs laser for producing microchannels. Chien et al. [8] compared the line cutting of silicon and stainless steel using a Ti:sapphire laser in its fundamental and second harmonic wavelengths of 800 nm and 400 nm, respectively, with pulse durations varying from 110 fs to 10 ps. Jia et al. [13] showed the effects of laser ablation with 115 fs pulses at 1040 nm wavelength on the physical and chemical properties of polylactide (PLA). Shibata et al. [14] demonstrated the biodegradability of a polymeric material, poly lactic-*co*-glycolic acid (PLGA), using 100 fs pulses at different wavelengths (400 nm and 800 nm). Guo et al. [15] discussed theories, methods, measurements, and applications of ultrafast lasers to micro/nano-machining.

Another aspect of ultrafast lasers is that extremely high intensity can be readily achieved with ultrashort pulses, resulting in nonlinear laser-material interactions such as self-focusing, filamentation, intensity rings around the filament and self-phase modulation (SPM). Ring-shaped damages on the surface of the material and voids at different points on a cross-sectional plane, which are observed for polypropylene (PP) sheets in our study, may be attributed to the intensity rings and multifilamentation respectively. The original laser pulse can break into multiple filaments when the power of the pulse exceeds the critical power (P_{cr}) for self-focusing.

The peak power of the pulse in our study varies from 5.88 to 588 MW which is much higher than the P_{cr} of the PP plastic sheets assuming that the P_{cr} of PP is a few MW. This is a reasonable assumption since four different plastics have P_{cr} in the range 0.8 – 2 MW based on calculations using Tamer's et al. [16] data on the nonlinear refractive indices (n_2) at

E-mail address: akar@creol.ucf.edu (A. Kar).

https://doi.org/10.1016/j.optlastec.2022.108886
Received 4 August 2022; Received in revised form 9 September 2022; Accepted 3 November 2022

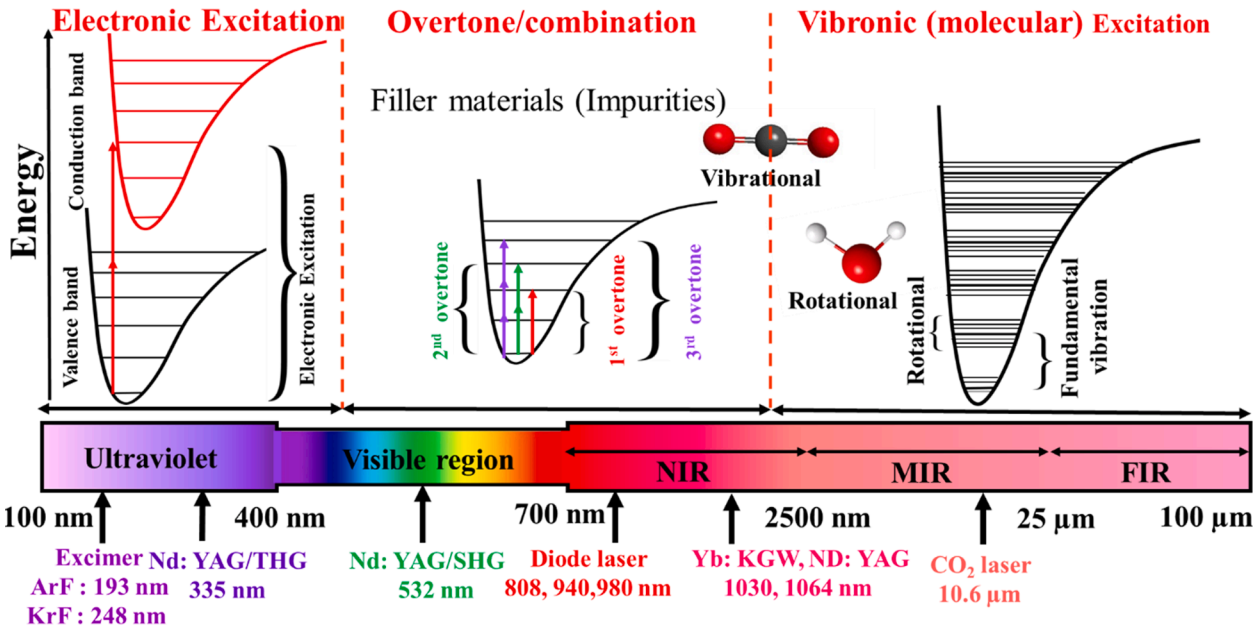

Fig. 1. Schematics of laser energy absorption by polymers in different spectral ranges.

1030 nm wavelength. In addition, D'Amore et al. [17] reported that the P_{cr} of polymethyl methacrylate (PMMA) sheets is 2–3 MW at 1500 nm wavelength.

The power of the pulse, however, varies as the pulse rises and falls in time at the leading and trailing edges respectively. This time-varying power influences the nonlinear interactions as the pulse traverses the material. If the pulse is considered a sequence of thin temporal slices, the pulse can be divided into three major slices with (i) the central temporal slice around the peak power and the weaker (ii) leading and (iii) trailing edges. The intense central slice is focused to a shorter distance than the other two temporal slices and this focal point defines the starting point of the filament [18,19]. So, the trailing edge of the pulse experiences aberrational defocusing, resulting in the formation of intensity rings around the filament [20]. The filament, which is initiated by the self-focusing of the central temporal slice of the pulse, splits into multiple filaments in the transverse plane of the laser beam [21–23]. Transverse modulational instability in the intensity generally causes multi-filamentation in materials with cubic nonlinearity. This instability emerges from the intensity perturbation such as the fluctuations of refractive index, the scattering of light by particles in the material, and the quality of output laser beam, i.e., the perturbation in the intensity distribution profile at the output of the laser system.

The above-mentioned self-focusing occurs when the Gaussian laser beam, which has a nonuniform transverse intensity distribution, creates a nonuniform transverse refractive index profile that modifies the shape and spatial structure of the beam. The temporal intensity distribution of the beam, on the other hand, causes a spectral nonlinear optical effect called the self-phase modulation (SPM). This nonlinear process arises from the Kerr nonlinearity when the ultrashort pulse modifies the refractive index. The time-varying refractive index induces phase shift in the pulse, resulting in spectral broadening with different frequency shifts in the above-mentioned three temporal slices of the ultrashort pulse. The leading-edge shifts to lower frequencies (red shift), trailing edge to higher frequencies (blue shift) and central slice to an approximately linear frequency shift (chirp, i.e., a temporal variation of the instantaneous frequency). Tamer et al. [16] reported spectral broadening due to SPM in four different types of plastics. Kudryashov et al. [24] measured spectral broadening, observed both the red- and blue-shifted frequencies, and analyzed the related SPM effect in CaF2. The purpose of applying the principle of SPM to two PP samples in our study is to show that a frequency of the broadened spectrum may correspond to a resonant absorption peak of the original material, and that this alignment of the broadened frequency to an absorption peak may preferentially select a particular order for multiphoton absorption.

Since nonlinear absorption becomes significant at high intensities, materials of very low linear absorption at the near-infrared wavelengths can be processed with ultrafast near-infrared lasers by utilizing the nonlinear optical properties of materials. Our previous work [25] presented both experimental and theoretical studies to understand the effect of laser parameters on ultrafast laser interaction with PP sheets. Polyakov et al. [26] demonstrated that multiple multiphoton absorption mechanisms contributed to the nonlinear absorption in Polydiacetylenes at most wavelengths from 1.2 to 2.2 um. Viertel et al. [27] used a fs laser of wavelength 1030 nm and noted electronic transition by four-photon absorption to excite electrons from the valence band to the conduction band for their material, polylactide, of bandgap 4.8 eV. The absorption mechanism in ultrafast laser interactions with polymeric materials, however, is unclear in the near-infrared (NIR) wavelengths since most polymers have high bandgaps and the energy of a NIR photon is too low to induce electronic transition in a single photon absorption process, but the low energy photons can be absorbed in the polymers by the fundamental molecular excitation mechanism.

Fig. 1 illustrates various modes of absorption such as electronic, vibrational and rotational transitions in polymers at different wavelengths. Typical polymers have very high bandgaps, for example, 6.9 eV for Polyethylene (PE) and 7.0 eV for polypropylene (PP) [28]. An UV laser of wavelength 335 nm corresponds to a photon of energy 3.7 eV and this wavelength is the third harmonic of a NIR laser of fundamental wavelength 1064 nm and photon energy 1.16 eV. At least 2-photon absorption of the UV laser would be required to induce electronic transitions in both PE and PP. For the NIR laser, on the other hand, electronic transitions would require at least 6-photon absorption in PE and PP. Since the probability of low order multiphoton excitation is higher than the probability of high order multiphoton excitation, the interactions between UV lasers and polymers are expected to occur via electronic transitions as presented in Fig. 1. Owing to lower photon energies in NIR lights, the NIR lasers can interact with polymers via vibrational excitation [29] as shown Fig. 1. For example, two photons are absorbed to transfer an electron from the valance band to the conduction band when a laser of wavelength 355 nm is used to process

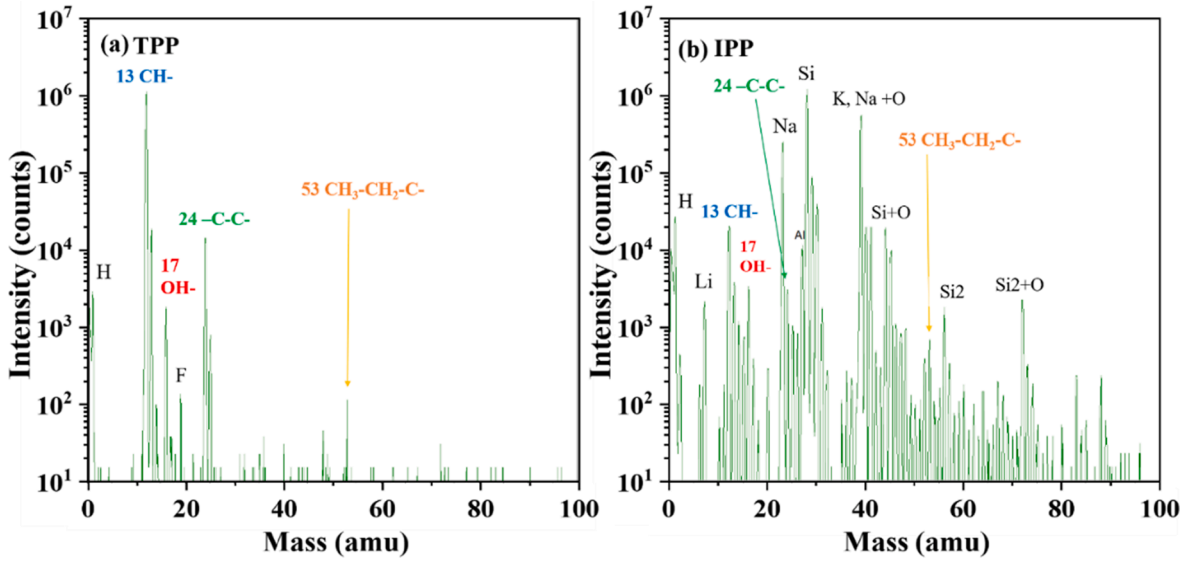

Fig. 2. Characteristic peaks of different elements in the secondary ion mass spectroscopic spectrum, (a) TPP sheet and (b) IPP sheet.

polypropylene as shown with red arrows in the UV region. The absorption of a light quantum changes the dipole moment of the molecule, causing a transition in the vibrational state. In general, light can be absorbed or emitted if the vibrational state jumps up or relaxes, respectively, corresponding to a change in the dipole moment of the molecule. In the far-infrared (FIR) region, the photon energies are much lower than in the NIR region and the dominant mechanism for the absorption of FIR lights is the rotational excitation of the molecules.

In the intermediate spectral range between the UV and FIR ranges, several phenomena contribute to the absorption of light in polymers. Many polymeric materials are transparent, indicating little absorption in the visible spectrum. The absorption, however, can be enhanced by adding impurities such as filler materials or color pigments into the material. The pigments can be organic or inorganic materials. Two other modes of absorption that contribute to weak absorption in the NIR region are vibrational overtones and combination excitation. The combination mode occurs when two or more molecular vibrations are excited simultaneously, and the overtone absorption involves the transitions of a molecule from its ground vibrational state to a higher vibrational state of the vibrational quantum number (V_q) more than or equal to 2. For example, the first and second overtones occur when the transitions are from $V_q = 0$ to $V_q = 2$ and $V_q = 0$ to $V_q = 3$ respectively.

Different impurities or pigments can enhance the vibrational overtone and the combination mode to increase the absorption of NIR lights in polymers. In addition, the absorption can be enhanced by inducing nonlinear absorption at high intensities of ultrafast NIR lasers. Fig. 1 indicates the absorption in the UV region for lasers obtained by the third harmonic generation (THG) of the fundamental 1030 nm wavelength. Similarly, in the visible spectrum, absorption occurs for lasers obtained by the second harmonic generation (SHG) of the fundamental 1030 nm wavelength.

Instead of the absorption of SHG and THG photons, the multiphoton absorption particularly 2-photon and 3-photon absorptions are studied in this paper for PP materials. PP is used in a wide range of applications including packaging for consumer products (medical industry), plastic parts for various industries (including automotive industry), and special devices like hinges, household products, battery cases, and fabrics [30]. Two types of samples, one of which is transparent polypropylene (TPP) and the other is impure polypropylene (IPP) since the sample contains certain additives.

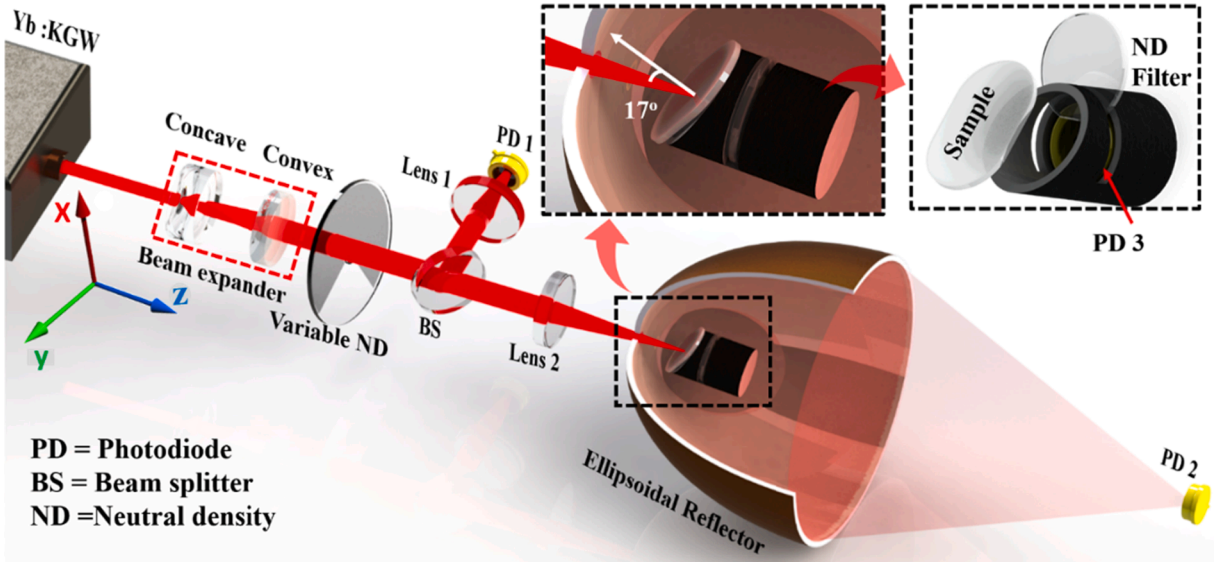

Fig. 3. Schematic of the experimental set up for measuring the reflectance and transmittance of IPP and TPP samples irradiated with one pulse of an ultrafast laser.

2. Characteristics of TPP and IPP

Different kinds of PP are commercially available, which can be broadly categorized into two groups based on optical properties, transparent polypropylene (TPP) and impure polypropylene (IPP) where the origin of various properties is ascribed to impurities in PP. However, the impurities induce the nonlinear absorption of ultrafast lasers differently compared to the nonlinearity in TPP. Fig. 2 shows the characteristic peaks of different elements in the secondary ion mass spectroscopic spectra for the TPP and IPP samples. The TPP sheet was 450 μm thick containing almost no impurity as indicated by its spectrum where C and C—C are dominant peaks.

The IPP sheet, which was 300 μm thick, exhibits peaks corresponding to several impurities Si, C, Li, Na, Al, K, and SiO_2 (Fig. 2b).

3. Measurements for determining absorptance

A Yb:KGW (Pharos, Light Conversion) femtosecond unpolarized laser of central wavelength $\lambda_0 = 1030$ nm is used in this study. Each sample is irradiated with a single pulse of duration 170 fs. The diameter of the output laser beam is 4 mm, which is enlarged and collimated to a 10 mm beam with a beam expander consisting of a concave and a convex lens of focal lengths −50 mm and 100 mm, respectively. A variable neutral density (ND) filter of optical density varying from 0.04 to 4.0 is placed after the beam expander to regulate the pulse energy for varying the fluence. The collimated beam is split into two parts with a beam splitter of splitting ratio 6.5/93.5. 6.5 % of the beam is directed to a reference photodetector PD 1 for determining the incident pulse energy, and the rest of the beam is focused onto a TPP or IPP sheet with a lens of 250 mm focal length as shown in Fig. 3. The diameter of the beam on the sample surface is measured to be 36.8 μm at $1/e^2$-point.

The surface of the sheet is placed at the first focal point of an ellipsoidal reflector (E180, Optiforms) using a sample holder. This holder is mounted on a 3D stage to move the sample for irradiating fresh spots on its surface with each laser pulse. By placing a photodetector PD 2 at the second focal point of the reflector, most of the light which is reflected off the sample due to both specular and diffusive reflections [31,32] is captured for determining the reflected laser power from the temporal response of PD 2. The loss of backscattered light through the entrance hole of the reflector is reduced by tilting the sample to have obliquely incident laser beam on the sample. The angle of incidence is 17° in this study, which enables the ellipsoidal reflector to direct the specularly reflected light toward PD 2. In addition, the reflector reflects most of the light, which is originally scattered diffusively by the sample, onto PD 2 and thus the loss of light that occurs due to the blocking of light by the sample, sample holder and 3D stage is reduced. A ZemaX ray tracing simulation indicates that the loss of reflected power at PD 2 is less than 1 %. The power of the light that transmits through the sample is determined from the temporal response of a photodetector PD 3 which is placed behind the sample. In the case of TPP samples, a 0.5'' ND filter of optical density 2 is placed in front of PD 3 to avoid saturating the photodetector.

The time constants of the three photodiodes (PD 1–3, Thorlabs, FDS100) are 1 ns, 1.2 ns and 1.1 ns, respectively, which are much higher than 170 fs pulse width of the laser used in this study. The temporal response of each photodetector is acquired with a 1-GHz oscilloscope (Tektronics, MD03104) and these data are analyzed using calibrated temporal response of oscilloscope to determine the reflectance *R*, transmittance *T*, and absorptance *A*. The details of this analysis are discussed elsewhere [33]. At low intensities of the laser, the TPP samples transmit most of the energy whereas the IPP samples mostly reflect and absorb the energy. The analysis of absorptance to examine the nonlinear absorption in TPP and IPP is the primary focus of this study.

4. Model for multiphoton excitation characteristics

The absorption mechanism during polymer processing with NIR wavelength is both linear (single photon) and nonlinear (multiphoton) processing [33,34] due to vibrational overtone or combination absorption [34]. Two models are discussed in this section, one of them is an intensity model and the second model is based on SPM theory. The intensity model provides a theoretical framework for determining the multiphoton excitation order by fitting the theoretical absorptance to experimental data. This model is briefly reviewed here since it has been discussed elsewhere [35].

4a. Intensity model:

The ultrafast laser pulse, which is incident on the sample, is considered to vary both spatially and temporally as given below:

$$I_{OI}(r_o, 0, t) = I_o e^{-\frac{2r_o^2}{w_o^2}} e^{-\frac{(4\ln 2)t^2}{t_{on}^2}} \tag{1}$$

where w_o is the radius at the waist of the laser beam and t_{on} is the pulse duration which is taken as the full-width at half-maximum of a Gaussian pulse. The peak intensity, $I_o = \frac{4E}{\pi w_o^2 t_{on}}$.

The laser intensity $I(r_i, z_i, t)$ is given [35] by Eq. (2), which describes the attenuation of the intensity due to single photon, 2-photon and 3-photon absorption as well as multiple reflections inside the material. This intensity model is based on a few assumptions. The electric field enhancement [36] at the back surface of the sample is ignored in Eq. (2) since this enhancement is negligible when the absorption coefficients are small for weakly absorbing media. Also Eq. (2) would be applicable when the geometrical thickness of the sample is much less than the coherence length of the laser inside the material [37]. The coherence length, $l_c = \lambda_o^2/(n\Delta\lambda)$, of the femtosecond laser of this study varies from 23.7 to 71.2 μm which is much smaller than the sample thickness, L = 450 μm, here n is the refractive index of the sample and $\Delta\lambda$ is the wavelength shift The samples are, therefore, considered to be optically thick and Eq. (2) is applicable to the present case. The optical properties of the polymer, however, change rapidly with time as the energy of the femtosecond laser pulse is deposited in the material. A dynamic process is thus established in the system where the leading edge of the pulse would encounter an unexcited material with a certain dielectric function or absorption, the trailing edge would encounter a highly excited material with a different dielectric function or absorption, and chirping would occur due to the central temporal slice of the pulse. These phenomena will set the linear and nonlinear absorption coefficients as functions of time. In addition, SPM would cause spectral broadening, resulting in frequency-dependent refractive indices. Also, multifilamentation breaks the original beam into multiple beams, which is ignored in this model. Since implementing these effects in a model is quite complicated, a simple model is considered for the intensity distribution as given by Eq. (2) and the solution of this equation is used to determine the effective nonlinear refractive indices.

$$\frac{dI_i(r_i, z_i, t)}{dz_i} = -\alpha_1 I_i(r_i, z_i, t) - \alpha_2 {I_i}^2(r_i, z_i, t) - \alpha_3 {I_i}^3(r_i, z_i, t) \tag{2}$$

where α_1, α_2 and α_3 are the linear, 2-photon and 3-photon absorption coefficients, respectively, and 2 and 3 are referred to as the nonlinear excitation order in this study. α_2 and α_3 generally represent the nonlinear absorption coefficients which are related to the imaginary part of the refractive index [38] as discussed in the Appendix. r_i and z_i in Eq. (2) are the radial and axial coordinates, respectively, for the i-th path of the laser beam inside the material, where $i = 1, 2, 3, \cdots$ and the z_i axis represents the direction of the laser beam propagation.

Eq. (2) is sequentially applied to determine the intensity $I_1(r_1, z_1, t)$ along the path R_0T_1 for i = 1 under the boundary condition given by $I_{OT}(r_o, 0, t)$ at R_0, $I_2(r_2, z_2, t)$ along the path T_1R_1 for i = 2 under the boundary condition given by $I_1(r_1, L_1, t)$ at T_1, and so on. For the intensities $I_1(r_1, z_1, t)$ and $I_2(r_2, Z_2, t)$ along the paths R_0T_1 and T_1R_1,

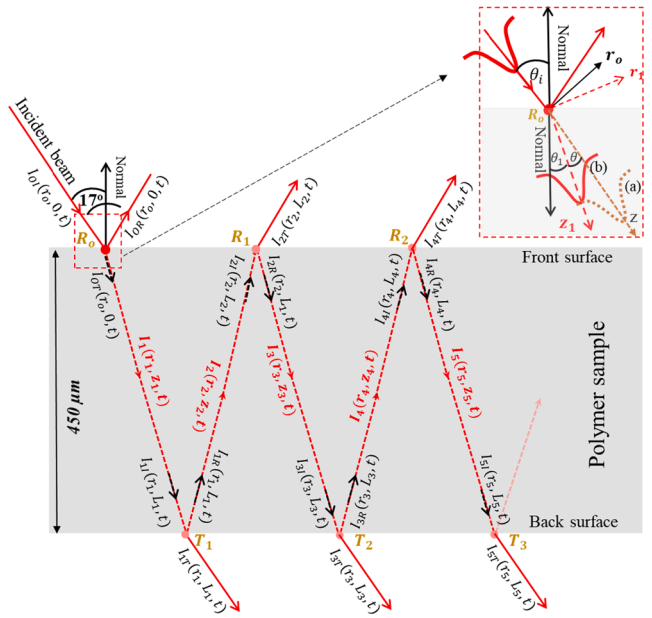

Fig. 4. Geometric configuration for the intensity model, showing the incident, reflected and transmitted intensities at various locations on the front and back surfaces, such as $(r_o, 0)$, (r_1, L_1), (r_2, L_2), …, and the direction of the laser beam propagation along various directions, such as $(r_1, 0)$, (r_1, z_1), (r_2, z_2), …, inside the material. Inset showing the intensity distributions at the incident point in two coordinate systems: (a) Intensity profile of the original beam at the coordinate system (r_o, z), and (b) Intensity profile of the transmitted beam at the coordinate system (r_1, z_1).

respectively, the specific forms of Eq. (2) and their boundary conditions are presented in the Appendix. Since the boundary conditions depend on the reflectance of the medium, the reflectance for unpolarized light at small (17° in this study) angles of incidence [38] is also analyzed in the Appendix. The transmitting beam along R_oT_1 (Fig. 4) and the original incident beam at R_o are in the (r_1, z_1) and (r_o, z) coordinate systems as illustrated with an inset in Fig. 4. To represent the intensity profile in the proper radial direction when the transmitted laser beam propagates along the direction R_0T_1, the intensity profile of the incident beam is transformed from the original coordinate system (r_o, z) to the transmitted coordinate system (r_1, z_1) using the following coordinate transformation matrix with the angles θ, θ_i and θ_1 shown by the inset in Fig. 4.

$$\begin{pmatrix} z \\ r_o \end{pmatrix} = \begin{pmatrix} cos\theta sin\theta \\ cos\theta - sin\theta \end{pmatrix} \begin{pmatrix} z_1 \\ r_1 \end{pmatrix}$$

$$\theta = \theta_i - \theta_1 \quad \theta_1 = \sin^{-1}\left(\frac{\sin(\pi\theta_i/180)}{n}\right) \quad \theta_i = 17^o \tag{3}$$

Under the boundary condition (A3), the solution of Eq. (2), or equivalently Eq. (A1), yields the intensity of the beam, $I_1(r_1, z_1, t)$, along R_oT_1. This solution is used to determine I_{1l} (r_1, L_1, t) which now represents the incident intensity at point T_1 and generates a boundary condition (A4) for solving Eq. (2), or equivalently Eq. (A2), to analyze the intensity of the beam, $I_2(r_2, z_2, t)$, along T_1R_1. Here the incident beam at T_1 and the transmitting beam T_1R_1 are in the (r_1, z_1) and (r_2, z_2) coordinate systems respectively. Therefore, the coordinate transformation matrix is applied to express all variables in the (r_2, z_2) coordinate system and Eq. (2), or equivalently Eq. (A3), is solved to determine $I_2(r_2, z_2, t)$. This procedure is continued to obtain the intensities along other directions such as R_1T_2, T_2R_2, R_2T_3, ….

The solution of Eq. (2) yields the following expression for the laser intensity incident at various points on the inner surfaces, $I_{il}(r_i, L_i, t)$, during the propagation of the beam inside the material:

$$I_{il}(r_i, L_i, t) = \frac{1}{3a_i(r_i, L_i, t)}\left(Q_i(r_i, L_i, t) + \frac{\Delta_{oi}(r_i, L_i, t)}{Q_i(r_i, L_i, t)} - b_i(r_i, L_i, t)\right) \tag{4}$$

All the variables in the above equation are defined in elsewhere [35]. The intensity of the transmitted beam, $I_{iT}(r_i, L_i, t)$, at each transmission point on the back surface can be determined using Eq. (4). At point T_1, for example, $I_{1T}(r_1, L_1, t)$ would be the product of $I_{1l}(r_1, L_1, t)$ and transmittivity. The total intensity due to all the transmitted beams, $I_T(r, z, t)$, at any arbitrary point (r, z) and time t on the back surface of the sample can be written as.

$$I_T(r, z, t) = \sum_{m=0}^{\infty} I_{(2m+1)T}(r_{(2m+1)}, L_{(2m+1)}, t) \tag{5}$$

where m = 0, 1, 2, 3 …, corresponding to the transmission points T_1, T_2, T_3, … (Fig. 4). Similarly, Eq. (4) can be applied to determine the intensity of the transmitted beam at various points R_1, R_2, … on the front surface of the sample (Fig. 4). These transmitted beams, however, add up with the reflected beam of the original incident laser and manifest as the total reflected intensity, $I_R(r, z, t)$, given by the following expression:

$$I_R(r, z, t) = I_{OR}(r, 0, t) + \sum_{m=1}^{\infty} I_{(2m)T}(r_{(2m)}, L_{(2m)}, t) \tag{6}$$

where m = 1, 2, 3 …, corresponding to the transmission points R_1, R_2, R_3, …. The intensity of the second transmitted beam is much smaller (<1%) than the first transmitted beam in this study and, therefore, the value of m is taken as 0 and 1 in both Eqs. (5) and (6), respectively. The absorptance, A, of the sample is determined from Eq. (7) utilizing the intensities given by Eqs. (5) and (6).

$$A = 1 - \frac{I_T(r, z, t)}{I_{OI}(r, 0, t)} - \frac{I_R(r, z, t)}{I_{OI}(r, 0, t)} \tag{7}$$

4b. Self-phase modulation model:

The wavelength of the incident laser shifts by the self-phase modulation (SPM) mechanism during the propagation of high intensity pulsed lasers through a nonlinear medium. The temporal phase change due to SPM gives rise to time-dependent angular frequency, $\omega(t)$, defined as

$$\omega(t) = \frac{d\varphi(t)}{dt} \tag{8}$$

where the temporal phase $\varphi(t) = \omega_o t - k_o n(t) z$. $\omega_o = 2\pi c/\lambda_0$ and $k_o = 2\pi/\lambda_0$ are the time-independent angular frequency and angular wavenumber, respectively, and c is the speed of light in vacuum. z is the axial distance inside the sample and this distance is measured in the direction of the laser beam propagation (Fig. 4). $n(t)$ is the time-dependent nonlinear refractive index which can be written as follows for nonlinear excitations of order up to 3.

$$n(t) = n_1 + \Delta n = n_1 + n_2 I(t) + n_3 I^2(t) \tag{9}$$

Here n_1 is the time-independent linear refractive index, and $n_2 and n_3$ are the second order and third order nonlinear refractive indices respectively. The spectral broadening during STM shifts the frequency of the original laser and, therefore, the frequency-dependent refractive index would govern the pulse propagation. Since the functions $n_1(\omega)$, $n_2(\omega)$, and $n_3(\omega)$ are unknown, the refractive indices are considered constant in Eq. (9) and in the intensity model (Eq. (2)) to simplify the nonlinear absorption analysis for estimating the nonlinear refractive indices.

Substituting $n(t)$ and $\varphi(t)$ into equation (8),

$$\omega(t) = \omega_o - \frac{2\pi}{\lambda_o} n_2 z \frac{dI(t)}{dt} - \frac{4\pi}{\lambda_o} n_3 z I(t) \frac{dI(t)}{dt} \tag{10}$$

where $\omega(t) = \frac{2\pi c}{\lambda(t)}$ is the instantaneous angular frequency, $\lambda(t)$ is the corresponding instantaneous wavelength of the laser and $dI(t)/dt$ is the

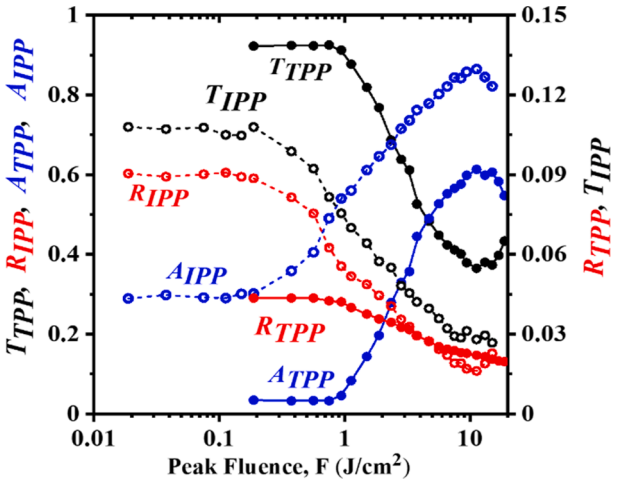

Fig. 5. Reflectance, transmittance, and absorptance R_{TPP}, T_{TPP}, and A_{TPP}, for TPP sample and R_{IPP}, T_{IPP}, and A_{IPP} for IPP sample, respectively, as a function of laser fluence F.

slope of the temporal laser pulse. Eq. (10) yields the following expression for the instantaneous wavelength $\lambda(t)$:

$$\lambda(t) = \frac{\lambda_o}{1 - \frac{n_2 z}{c}\frac{dI(t)}{dt} - \frac{2n_3 z I(t)}{c}\frac{dI(t)}{dt}} \tag{11}$$

Therefore, the shift in the wavelength can be written as

$$\lambda(t) - \lambda_o = \lambda_o \left(\frac{n_2 \frac{dI(t)}{dt} + 2n_3 I(t)\frac{dI(t)}{dt}}{\frac{c}{z} - n_2 \frac{dI(t)}{dt} - 2n_3 I(t)\frac{dI(t)}{dt}} \right) \tag{12}$$

Since the magnitude of the intensity slope $dI(t)/dt$ is typically very large for ultrashort laser pulses, the wavelength of the laser is expected to vary inside the material during laser-matter interactions. Consequently, the mechanism of laser absorption may shift from low absorption or nonresonant interactions to high absorption or resonant interactions. This type of shift in the absorption mechanism can be utilized to explain whether 2-photon, 3-photon or *n*-photon absorption would preferentially occur as discussed in section 5b.

5. Results and discussion

The experimental studies yield two classes of results: optical properties of TPP and IPP, and physical damage in the materials. The intensity model is utilized to extract the nature of nonlinear absorptions in these two materials, and the SPM model is applied to explain the difference in the multiphoton excitation order.

5a. Optical properties and nonlinear absorption:

The experimental values of total (specular and diffusive) reflectance for TPP (R_{TPP}) and IPP (R_{IPP}), and the corresponding transmittances T_{TPP} and T_{IPP} are presented in Fig. 5. These results are obtained from the integrated areas at the full-width half-maximum of the PD traces acquired with an oscilloscope operating at 1 GHz, and the details of this procedure can be found in Ref. [35]. Using the relationship that the sum of reflectance, transmittance and absorptance is unity, the absorptances of TPP (A_{TPP}) and IPP (A_{IPP}) are determined as shown in Fig. 5.

Fig. 5 shows that the reflectances,R_{TPP} and R_{IPP} are constant at approximately 0.044 and 0.6, respectively. Similarly, the transmittance and the absorptance are constant up to a certain fluence F. This constant F region is designated as the linear absorption region in this study and the laser does not damage the material in this region. Physical damages of the materials are discussed in section 5c.

As F increases, however, the reflectance and transmittance decrease due to nonlinear absorption. The reflectance and transmittance vary

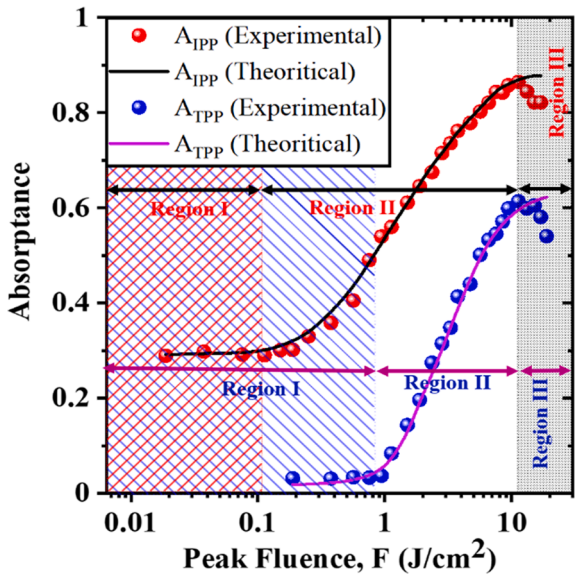

Fig. 6. Results of the intensity model fitted to the experimental data for determining the linear and nonlinear absorption coefficients of IPP and TPP samples.

nonmonotonically at very large fluences, $F > 10$ J/cm^2 and the absorptance decreases with increasing F. The absorptance is found to be much higher in IPP than TPP for all the three, low, medium and large fluence regions and this trend is ascribed to the impurities present in the IPP material. These three regions are denoted as region I, region II, and region III in Fig. 6.

The linear absorption dominates in Region I where the absorptance is nearly constant up to a certain peak fluence *F,* which are 0.15 J/cm^2 and 0.94 J/cm^2 for IPP and TPP, respectively. The absorptance increases as F increases in Region II, indicating the occurrence of nonlinear absorption in this region. When F is increased further, however, the absorptance decreases in region III. This anomalous absorption may be attributed to several effects such as the breakdown of the atomic bonds in the materials, resulting in new damaged phases compared to the original polymeric structures. The damaged phases can increase the reflectance or transmittance, or increase both the reflectance and transmittance, and thus lower the absorptance. It is evident in Fig. 5 that the reflectance and transmittance have increased in Region III for the IPP and TPP samples, respectively. Another plausible explanation of the anomalous absorption could be that the damaged phases scatter the laser pulse, resulting in a distorted intensity profile both in the spatial and temporal dimensions. The scattered beam can cause speckle interferometric patterns with various slopes of the intensity with respect to time. These slopes would give rise to different spectral phase modulations that can vary the absorptance.

Regions I and II are analyzed further using the intensity model presented in section 4a, particularly Eq. (9) is fitted to the experimental data as shown in Fig. 6 for extracting the multiphoton excitation order and the values of the absorption parameters. For the TPP sample, the average value of the linear absorption coefficient α_1 is found to be $\alpha_1 = 110.45 \pm 3$ m^{-1}, and this value compares well with the experimental data ($\alpha_1 = 109$ m^{-1}) determined from the absorption spectrum measured with a spectrophotometer. The multiphoton excitation order is up to 3 for this sample and the corresponding nonlinear absorption coefficients are found to be $\alpha_2 = (8.01 \pm 2.15) \times 10^{-13}$ mW^{-1} for 2-photon absorption and $\alpha_3 = (3.21 \pm 1) \times 10^{-29}$ m^{3}W^{-2} for 3-photon absorption, respectively. Heberle et. al [39] and Rafique et. al [40] reported the three-photon absorption coefficients of two other polymers as α_3 on the order of $10^{-29} m^3 W^{-2}$ for a laser of wavelength 1064 nm, and the result for the TPP of current study is consistent with their results. The

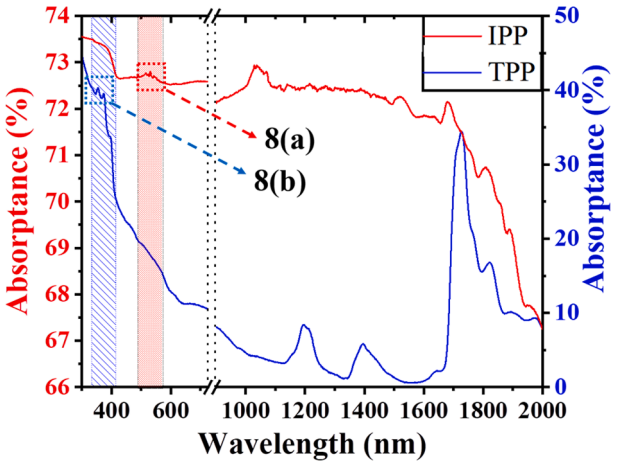

Fig. 7. Linear absorption spectrum for IPP (top) and TPP (bottom), showing tiny absorption peaks at wavelengths much lower than 1030 nm.

nonlinear refractive indices of the TPP sample are found to be, $n_1 = 1.49$, $n_2 = (3.22 \pm 1.15) \times 10^{-20}$ m^2W^{-1} and $n_3 = (2.64 \pm 1) \times 10^{-37}$ m^4W^{-2}. For the IPP sample, on the other hand, 3-photon was found to be absent and the linear and 2-photon absorption coefficients are found to be $\alpha_1 = 5269$ m^{-1} and $\alpha_2 = 1.391 \times 10^{-12}$ mW^{-1}, respectively, with corresponding refractive indices as $n_1 = 1.44$ and $n_2 = (1.69 \pm 0.95) \times 10^{-19}$ m^2W^{-1}, respectively.

5b. Effect of SPM:

To understand the difference in the multiphoton excitation order of the IPP and TPP samples, the absorption spectra of these two samples are analyzed using the SPM model of section 4b. The spectra (Fig. 7) are obtained using a spectrophotometer at room temperature and they represent the linear absorption regime since the spectrophotometer uses a low intensity light source. While Fig. 7 provides an overview of the spectra for a broad spectral range, Fig. 8a and 8b show the details of certain absorption peaks since these peaks play a role in modifying the absorption mode to 2-photon or 3-photon depending on how the wavelength of the original laser is shifted by the SPM phenomenon. Figs. 7 and 8a indicate nonresonant absorption around 1030 nm and a vibrational overtone/combination resonant absorption peak around 515 nm for the IPP sample, respectively, suggesting that 2-photon absorption may occur for this sample. For the TPP sample, on the other

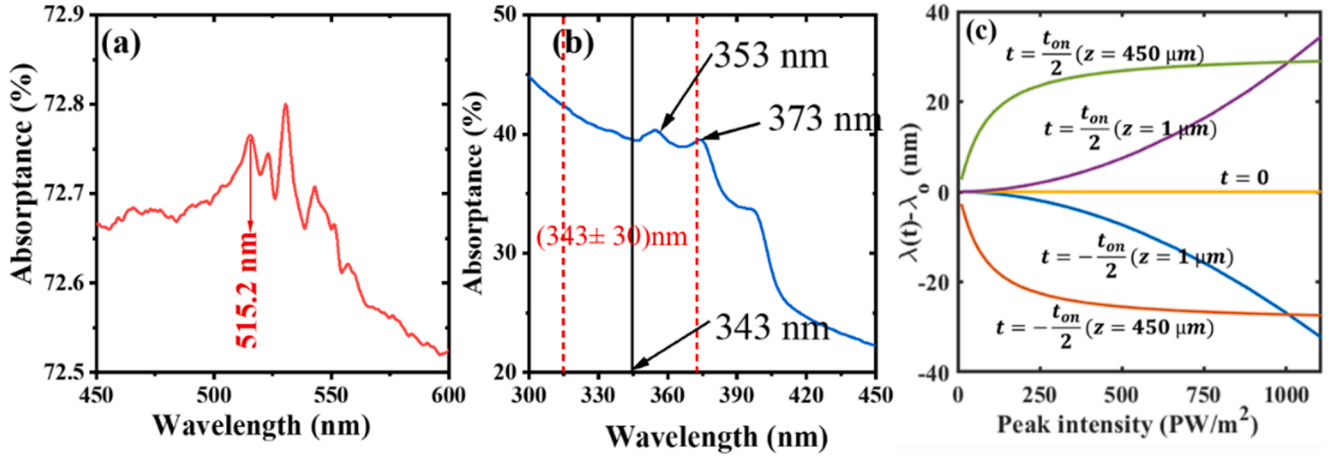

Fig. 8. (a) absorption peaks of IPP near the second harmonic of 1030 nm wavelength, (b) absorption peaks of TPP near the third harmonic of 1030 nm wavelength, and (c) wavelength shift in TPP at various times as the laser pulse rises and falls causing a variation in the intensity of the pulse.

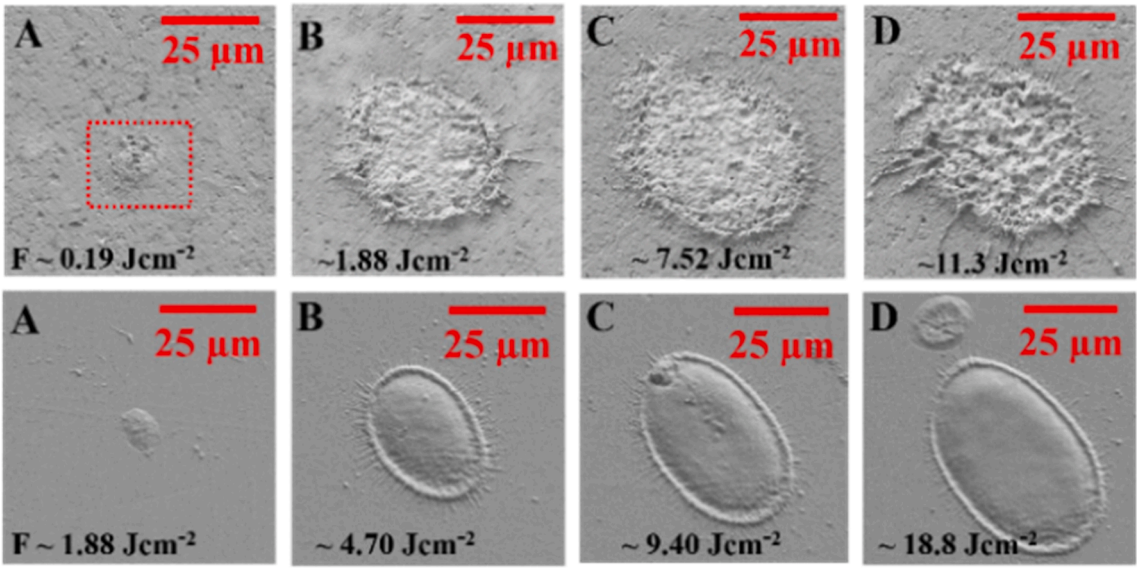

Fig. 9. SEM images of damages at the top surface of IPP (top row) and TPP (bottom row) for different fluences.

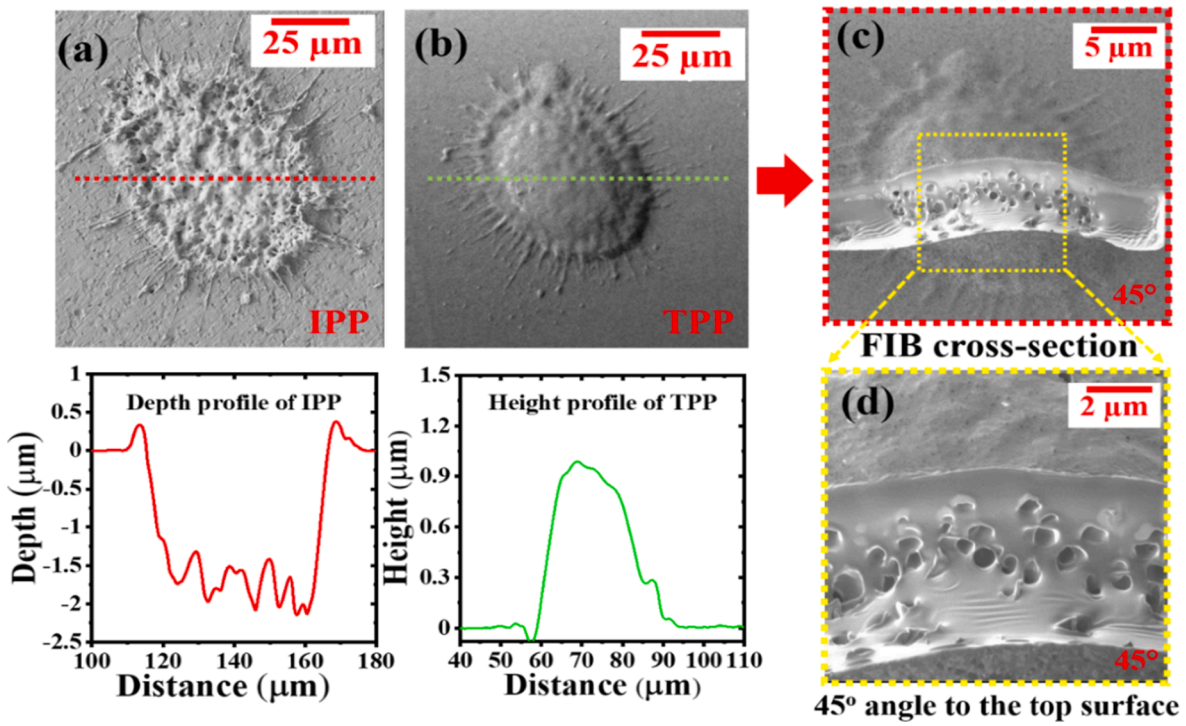

Fig. 10. (a) SEM image of the damage and damage profile at the surface of IPP, (b) SEM image of the damage and damage profile at the surface of TPP and (c, d) Cross-sectional analysis by focused ion beam (FIB) milling of the TPP sample shown in (b).

hand, Fig. 7 shows nonresonant absorption around 1030 nm and 515 nm, and Fig. 8b exhibits a vibrational overtone /combination resonant absorption peak around 353 nm, suggesting that 3-photon absorption is more dominant than 2-photon absorption.

To analyze the role of SPM on absorption mode, Eq. (12) is used to calculate the shift in the wavelength (Dl) of the original laser for different peak intensities at different depths inside the TPP sample. Fig. 8c shows the variation of Dl as a function of the peak intensity at different times during the laser pulse, $t = -t_{on}/2$, $t = 0$ and $t = +t_{on}/2$, and at different distances,$z = 1$ μm and $z = 450$ μm along the direction of the laser beam propagation.

In this study, the coherence length, $l_c = \lambda_o^2/(n\Delta\lambda)$, varies from 71.2 to 23.7 μm corresponding to the wavelength shift, $\Delta\lambda = 10$ and 30 nm, respectively, due to the SPM mechanism. $Dl = \pm 10$ nm and $Dl = \pm 30$ nm occurs at the peak intensities 50 PW/m^2 and 1061 PW/m^2, respectively, and these wavelength shifts promote 3-photon absorption due to the presence of resonant absorption peaks (Fig. 8b) in the neighbourhood of the third harmonic (~343 nm) of the original laser wavelength (1030 nm). The resonant absorption peaks in Fig. 8b are at 353 nm and 373 nm. $Dl = +10$ nm and $Dl = +30$ nm will, therefore, shift the third harmonic wavelength ~ 343 nm to the resonant absorption wavelengths 353 nm and 373 nm, respectively, to induce 3-photon absorption. The electronic excitation can occur in TPP at these wavelengths as illustrated in Fig. 1. The IPP sample, on the other hand, exhibits an absorption peak at 515 nm (Fig. 8a), which is the second harmonic of the original laser wavelength. 2-photon absorption would, therefore, occur in the IPP sample as indicated by the results in section 5a.

5c. Physical damages:

The effect of 2-photon and 3-photon absorptions can be observed in the laser-induced damages to the IPP and TPP samples respectively. Since the probability of 2-photon absorption is higher than that of the 3-photon absorption, the laser is expected to damage IPP more than TPP. This difference in the damage is evident in Fig. 9. The scanning electron microscopy (SEM) images A, B, C and D in the top row of Fig. 9 show damages at the top surface of IPP for fluences $F = 0.19$, 1.88, 7.52, and 11.3 J/cm^2, respectively, and the SEM images A, B, C and D in the bottom row are for TPP at $F = 1.88$, 4.70, 9.40 and 18.8 J/cm^2, respectively. The damages in micrographs A of both samples were found to occur at the damage threshold fluence (F_{th}), and F_{th} is much lower for IPP than TPP due to more absorption of the light by IPP. The images B, C and D indicate that the damage size increases with the fluence.

Fig. 9 also shows that the damage morphologies are different for the two samples. Craters and dome-like structures are observed for IPP and TPP respectively. The depth of a typical crater and the height of a typical dome were measured with a profilometer (Dektak XT, Bruker), and the damage profiles are presented in Fig. 10(a) and 10(b). These damages occurred at the peak fluences 9.40 J/cm^2 and 3.76 J/cm^2 for the IPP and TPP samples respectively. The average depth of the crater in IPP is ~ 1.75 μm and the average height of the dome on TPP is ~ 1.0 μm. The formation of craters at high fluences can be attributed to instantaneous heating [41], resulting in localized melting, explosive boiling and micro/nano splashes. Low fluences, however, cause expansion [34,36] and thermal decomposition of the polymer, resulting in gases. The expansion of the solid polymer and the gases can create dome-shaped swelling [42–44] and micro/nano voids. The ring-shaped damages with a central elliptical disk surrounded by an elliptical ring on the surface of TPP samples in Fig. 9b-9d (bottom row in Fig. 9) and Fig. 10b may be due to the intensity rings that are formed around the filament during laser-matter nonlinear interactions as discussed in the introduction section. The elliptic shapes of the damaged spots may be ascribed to the oblique incidence of a circular laser beam on the surface.

The formation of voids near the surface of a TPP sample is confirmed by the cross-sectional analysis of the sample as shown in Fig. 10(c,d). The cross-sections were obtained by milling a TPP sample with a focused ion beam, and the results are presented at the view angle of 45° to the surface of the smaple. The sample was irradiated with a single femtosecond laser pulse of energy 20 μJ, peak fluence 3.76 J/cm^2 and pulse duration 170 fs. The average diameter of the voids increases with the irradiated pulse energy, yielding typical diameters of 0.2 and 3 μm corresponding to the pulse energies 12.5 μJ and 100 μJ respectively. Numerous voids at various points on a cross sectional plane in Fig. 10c are expected to be due to a nonlinear effect multifilamentation as

discussed in the introduction section. The voids may be due to STM as well. No void can be seen on the left and right sides of the sample in Fig. 10(c) since the sample surface was outside the irradiating laser spot. Fig. 10(d) shows the central portion of the irradiated region where the size of the voids is larger and also the density of the voids is higher. As the laser fluence increases, the size of the voids can be larger with higher density, resulting in more transmision and scattering of the laser beam inside the sample. These effects may be the contributing factor for the anomalous absorption, i.e., decreasing absorptance in Region III (Fig. 6).

6. Conclusions

The absorptance of two types of polypropylene samples, IPP and TPP, have been determined from the reflectance and transmittance data for a wide range of fluences to understand the absorption mechanisms of an ultrafast laser by the polymeric materials. The absorption mechanism in IPP is significantly different from that of TPP due to the presence of impurity in IPP. The impurity also modifies the spectrophotometric absorption spectrum of the initial IPP sample, exhibiting absorption peaks at certain wavelengths that are different from the spectrum of the initial TPP sample. The presence of these absorption peaks in the initial samples is found to affect the nonlinear absorption mechanisms. The laser can attain a new wavelength due to the self-phase modulation, resulting in enhanced absorption when the new wavelength coincides with one of the absorption peaks of the original sample. While two-step and/or two-photon absorption is found to be dominant in IPP, three-step and/or three-photon absorption occurs in TPP, and this higher order absorption fits the self-phase modulation model. A nonlinear absorption model is fitted to the experimental data on absorptance, and both the linear and nonlinear absorption coefficients are determined. Under the laser-polymer interactions, severe damages occurred in the IPP sample with significant thermal effects such as melting and vaporization, and the TPP sample showed swelling at the surface and micro/nano voids inside the material.

Declaration of Competing Interest

The authors declare that they have no known competing financial interests or personal relationships that could have appeared to influence the work reported in this paper.

Acknowledgments

The authors thank Dr. Xinpeng Du, and Boyang Zhou for their helpful discussion. The authors also thank Yingjie Chai for his support in SEM imaging. The authors appreciate Dr. Xiaoming Yu's assistances for the experimental data at his laboratory in CREOL.

Appendix

The laser intensities $I_1(r_1, z_1, t)$ and $I_2(r_2, z_2, t)$ along the lines R_oT_1 and T_1R_1, respectively, in Fig. 4 can be written as:

$$\frac{dI_1(r_1,z_1,t)}{dz_1} = -\alpha_1 I_1(r_1,z_1,t) - \alpha_2 {I_1}^2(r_1,z_1,t) - \alpha_3 {I_1}^3(r_1,z_1,t) \tag{A1}$$

$$\frac{dI_2(r_2,z_2,t)}{dz_2} = -\alpha_1 I_2(r_2,z_2,t) - \alpha_2 {I_2}^2(r_2,z_2,t) - \alpha_3 {I_2}^3(r_2,z_2,t) \tag{A2}$$

where the linear (α_1) and nonlinear (α_2, α_3) absorption coefficients are related to the linear (κ_1) and nonlinear (κ_2, κ_3) absorption indices by the expressions $\alpha_1 = (4\pi\kappa_1)/\lambda_0$, $\alpha_2 = (4\pi\kappa_2)/\lambda_0$, and $\alpha_3 = (4\pi\kappa_3)/\lambda_0$. These absorption indices define the intensity-dependent absorption index, $\kappa(I) = \kappa_1 + \kappa_2 I + \kappa_3 I^2$ for an arbitrary intensity I. Eqs. (A1) and (A2) can be solved under the following boundary conditions:

$$I_1(r_1,0,t) = I_{0T}(r_1,0,t) = [1 - R_o(I_{OI})]I_{OI}(r_o,0,t) \tag{A3}$$

$$I_2(r_2,L_2,t) = I_{1R}(r_1,L_1,t) = R_{1I}(I_{1I})I_{1I}(r_1,L_1,t) \tag{A4}$$

where $I_{0I}(r_0,0,t)$ and $I_{1I}(r_1,L_1,t)$ are the incident intensities at points R_0 and T_1 (Fig. 4), respectively, with L_1 as the length of the line R_0T_1. $R_0(I_{0I}(r_0,0,t))$ and $R(I_{1I}(r_1,L_1,t)$ are the intensity-dependent reflectivities at points R_0 and T_1 respectively. The reflectivity for the unpolarized laser beam of this study is taken as the average of the reflectivities R_{TE} and R_{TM} of the Transverse Electric (TE) and Transverse Magnetic (TM) polarized waves respectively. Therefore, the reflectivity at the first incident point R_0 is given by the following expression:

$$R_o(I_{OI}) = \frac{1}{2}(R_{TE} + R_{TM}) \tag{A5}$$

where $R_{TE} = |r_{TE}|^2$ and $R_{TM} = |r_{TM}|^2$ and r_{TE} and r_{TM} are the reflection coefficients of the TE and TM polarized waves respectively. For reflectivity at small angles [39] of incidence Eq. (A5) can be written as.

$$R_o(I_{OI}) = \frac{\{(n(I_{OI})-1)^2 + \kappa^2(I_{OI})\}}{\{(n(I_{OI})+1)^2 + \kappa^2(I_{OI})\}}\left(1 + \frac{\theta_i^4}{\{n^2(I_{OI}) + \kappa^2(I_{OI})\}}\right) \tag{A6}$$

where $n(I_{OI})$ is the intensity-dependent refractive index given by $n(I_{0I}) = n_1 + n_2 I_{OI} + n_3 I_{OI}^2$ with n_1 as the linear refractive index, and n_2 and n_3 as the nonlinear refractive indices. $\kappa(I_{OI})$ is the intensity-dependent absorption index which can be written as $\kappa(I_{OI}) = \frac{\lambda_0(\alpha_1 + \alpha_2 I_{0I} + \alpha_3 I_{OI}^2)}{4\pi}$. In our experiment, θ_i is 17^o, which indicates from Eq. (A6) that reflectivity at small angle is almost similar with normal angle incidence, i.e,

$$R_o(I_{OI}) \approx \frac{\{(n(I_{OI})-1)^2 + \kappa^2(I_{OI})\}}{\{(n(I_{OI})+1)^2 + \kappa^2(I_{OI})\}} \tag{A7}$$

Similarly, R_{1I} in the boundary condition (A4) is taken as the reflectivity under the normal incidence with the following expression:

$$R_{1I}(I_{1I}) \approx \frac{\left\{(n(I_{1I})-1)^2+\kappa^2(I_{1I})\right\}}{\left\{(n(I_{1I})+1)^2+\kappa^2(I_{1I})\right\}} \tag{A8}$$

References

[1] R. Srinivasan, E. Sutcliffe, B. Braren, Ablation and etching of polymethylmethacrylate by very short(160 fs) ultraviolet(308 nm) laser pulses, Appl. Phys. Lett. 51 (1987) 1285–1287.
[2] S. Kuper, M. Stuke, Femtosecond UV excimer laser ablation, Appl. Phys. B 44 (1987) 199–204.
[3] K. Sugioka, Y. Cheng, Ultrafast lasers - reliable tools for advance materials processing, Light Sci. Appl. 3 (2014) e149.
[4] R.S. Taylor, D.L. Singleton, G. Paraskevopoulos, "Optical fiber transmission in excimer laser angioplasty", Conference on Laser Electro-Optics (CLEO), OSA/IEEE, Baltimore, Maryland, 1987.
[5] B.N. Chichkov, C. Momma, S. Nolte, F.V. Alvensleben, A. Tunnermann, Femtosecond, picosecond and nanosecond laser ablation of solids, Appl. Phys. A 63 (1996) 109–115.
[6] I.H. Chowdhury, X. Yu, Heat transfer in femtosecond laser processing of metal, Numer. Heat transf. A 44 (2003) 219.
[7] X. Zhao, Y.C. Shin, Femtosecond laser drilling of high-aspect ratio microchannels in glass, Appl. Phys. A 104 (2011) 713.
[8] C.Y. Chien, M.C. Gupta, Pulse width effect in ultrafast laser processing of mateirals, Appl. Phys. A 81 (2005) 1257–1263.
[9] M. Malinauskas, A. Žukauskas, S. Hasegawa, Y. Hayasaki, V. Mizeikis, R. Buividas, S. Juodkazis, Ultrafast laser processing of materials: from science to industry, Light Sci. Appl. 5 (8) (2016) 1–14.
[10] L.L. Taylor, J. Xu, M. Pomerantz, T.R. Smith, J.C. Lambropoulos, J. Qiao, Femtosecond laser polishing a germanium, Opt. Express 9 (2019) 4165–4177.
[11] T. Ersoy, T. Tunay, M. Uğuryol, G. Mavili, S. Akturk, Femtosecond laser cleaning of histrorical paper with sizing, J. Cult. Herit. 15 (3) (2014) 258–265.
[12] J. Cheng, C.S. Liu, S. Shang, D. Liu, W. Perrie, G. Dearden, K. Watkins, Surface structure formation in WE54 Mg alloy subjected to ultrafast laser texturing, Opt. Laser Technol. 46 (2013) 88–102.
[13] W. Jia, Y. Luo, J. Yu, B. Liu, M. Hu, L. Chai, C. Wang, Effects of high-rate femtosecond laser micromachining on the physical and chemical properties of polylactide (PLA), Opt. Express 23 (21) (2015) 26932–26939.
[14] A. Shibata, S. Yada, M. Terakawa, Biodegradability of poly(lactic-co-glycolic acid) after femtoseond laser irradiation, Sci. Rep. 6 (2016) 27884.
[15] B. Guo, J. Sun, Y. Zhan, J. Jia, K. Chu, Femtosecond laser micro/nano-manufacturing: theories, measurements, methods, and applications, Nanomanuf. Metrol. 3 (2020) 26–67.
[16] I. Tamer, M. Hornung, L. Lukas, M. Hellwing, S. Keppler, R. Van Hull, J. Hein, M. Zepf, M.C. Kaluza, Characterization and application of nonlinear plastic materials for post-CPA pulse compression", Opt. Lett. 45 (2020) 6575–6578.
[17] F. D'Amore, M. Lanata, S.M. Pietralunga, M.C. Gallazzi, G. Zerbi, Enhancement of PMMA nonlinear optical properties by means of a quinoid molecule, Opt. Mater. 23 (4) (2004) 661–665.
[18] J.-P.-E. Taran, T.K. Gustafson, Comments on the self-focusing of short light pulses, IEEE J. Quant. Electron. 5 (1968) 381–382.
[19] A. Brodeur, C.Y. Chien, F.A. Ilkov, S.L. Chin, O.G. Kosareva, V.P. Kandidov, Moving focus in the propagation of ultrashort laser pulses in air, Opt. Lett. 22 (1997) 304.
[20] S.L. Chin, N. Akozbek, A. Proulx, S. Petit, C.M. Bowden, Transverse ring formation of a femtosecond laser pulse propagating in air, Opt. Commun. 188 (2001) 181–186.
[21] S. Tzortzakis, L. Berge, A. Couairon, M. Franco, B. Prade, A. Mysyrowicz, Breakup and fusion of self-guided femtosecond light pulses in air, Phys. Rev. Lett. 86 (2001) 5470–5473.
[22] B. La Fontaine, F. Vidal, Z. Jiang, C.Y. Chien, D. Comtois, A. Desparois, T. W. Johnston, J.-C. Kieffer, H. Pepin, Filamentation of ultrashort pulse laser beams resulting from their propagation over long distances in air, Phys. Plasmas 6 (1999) 1615–1621.
[23] V.P. Kandidov, A.E. Dormidonov, O.G. Kosareva, S.L. Chin, W. Liu, The effect of the beam quality on the filamentation of high-power femtosecond laser pulses in air, Bull. Russ. Acad. Sci. Phys. 66 (2002) 1091–1102.
[24] S. Kudryashov, P. Danilov, A. Rupasov, S. Khonina, A. Nalimov, A. Ionin, G. Krasin, M. Kovalev, et al., Energy deposition parameters revealed in the transition from 3D to 1D femtosecond laser ablation of fluorite at high-NA focusing, Opt. Mater. Express 10 (2020) 3291–3305.
[25] A. Rahaman, A. Kar, X. Yu, Thermal effects of ultrafast laser interaction with polypropylene, Opt. Express 27 (4) (2019) 5764–5783.
[26] S. Polyakov, F. Yoshino, M. Liu, G. Stegeman, Nonlinear refraction and multiphoton absorption in polydiacetylenes from 1200 to 2200 nm, Phys. Rev. B 69 (2004), 115421.
[27] T. Viertel, L. Pabst, M. Olbrich, R. Ebert, A. Horn, H. Exner, Generation of nano-voids inside polylactide using femtosecond laser radiation, Appl. Phys. A 123 (2017) 789.
[28] Y. Ohki, N. Fuse, T. Arai, "Band gap energies of several insulating polymers estimated by optical absorption", 2010 Annual Report Conference on Electrical Insulation and Dielectic Phenomena, West Lafayette, IN, USA, 2010, pp. 1–4.
[29] D.D. Dlott, Ultrafast vibrational energy transfer in the real world: laser ablation, energetic solids, and hemeproteins, J. Opt. Soc. Am. A: 7 (1990) 1638–1652.
[30] H.A. Maddah, Polypropylene as a promising plastic: A Review, Am. J. Polym. Sci. 6 (1) (2016) 1–11.
[31] A.Y. Vorobyev, C. Guo, Reflection of femtosecond laser light in multipulse ablation of metals, J. Appl. Phys. 110 (2011), 043102.
[32] O. Benavides, O. Lebedeva, V. Golikov, Reflection of nanosecond ND: YAG laser pulses in ablation of metals, Opt. Express 19 (22) (2011) 21842.
[33] A. Rahaman, A. Kar, X. Yu, Time-resolved measurements of optical properties in ultrafast laser interaction with polypropylene, Opt. Express 28 (2) (2020) 2640.
[34] M. Asobe, I. Yokohama, T. Kaino, S. Tomaru, T. Kurihara, Nonlinear absorption and refraction in an organic dye functionalized main chain polymer waveguide in the 1.5 μm wavelength region, Appl. Phys. Lett. 67 (7) (1995) 891.
[35] A. Rahaman, X. Du, B. Zhou, A. Kar, X. Yu, Pulse-to-pulse evolution of optical properties in ultrafast laser micro-processing of polymers, J. Laser Appl. 33 (2020) (012020).
[36] M.D. Crisp, N.L. Boling, G. Dube, Importance of Fresnel reflections in laser surface damage of transparent dielectrics, Appl. Phys. Lett. 21 (1972) 364.
[37] E. Nichelatti, Complex refractive index of a slab from reflectance and transmittance: analytical solution, J. Opt. A: Pure Appl. Opt. 4 (2002) 400–403.
[38] E. Hecht, Optics, Fifth Edition, Pearson Education Limited, 2017.
[39] J. Heberle, T. Häfner, M. Schmidt, Nonlinear absorption measurements of intraocular lens polymers by integrating Z-Scan, J. Laser Appl. 28 (2016), 022604.
[40] M.S. Rafique, S. Bashir, A. Ajami, W. Husinsky, Nonlinear absorption properties correlated with the surface and structural changes of ultra-short pulse laser irradiated CR-39, Appl. Phys. A 100 (2010) 1183–1189.
[41] F. Baset, A. Villafranca, J.M. Guay, R. Bhardwaj, Femtosecond laser-induced porosity in poly-methyl methacrylate, Appl. Sur. Sci. 282 (2013) 729.
[42] E.G. Gamaly, S. Juodkazis, H. Misawa, B.L. Davies, A.V. Rode, L. Hallo, P. Nicolai, V.T. Tikhonchuk, Formation of nano-voids in transparent dielectrics by femtosecond lasers, Appl. Phys. 8 (2008) 412.
[43] F. Baset, K.K. Popov, A. Villafranca, J.M. Guay, Z. Al-Rekabi, A.E. Pelling, L. Ramunno, R. Bhardwaj, Femtosecond laser-induced surface swelling in poly-methyl methacrylate, Opt. Express 21 (10) (2013) 12527.
[44] J. Li, W. Wang, X. Mei, X. Sun, A. Pan, The formation of convex microstructures by laser irradiation of dual-layer polymethylmethacrylate (PMMA), Opt. Laser Technol. 106 (2018) 461.